CHAPTER 12

Nanoscale Biological Fluorescence Imaging: Breaking the Diffraction Barrier

Travis J. Gould and Samuel T. Hess

Department of Physics and Astronomy and Institute for Molecular Biophysics
University of Maine
Orono, Maine 04469

Abstract
I. Introduction
  A. Observation Volume Confinement
  B. Modulated Illumination
  C. Hyperlens Imaging
  D. Single-Molecule Localization and Reconstruction
II. Theory and Rationale
III. Methods
  A. Choice of Probe
  B. Choice of Filters
  C. Alignment and Characterization of the Illumination Area
  D. Choice of Sample Region
  E. Position Stability
  F. Fluorescence Background
  G. Adjustment of Thresholds
  H. Rendering the Results
  I. Biological Applications in Live Cells
IV. Materials
V. Discussion
  A. Density of Localized Molecules
  B. Factors Which Can Bias the Measured Distribution of Molecules
  C. Failed Localization: Pixelization Artifacts
  D. Light Exposure

0091-679X/09 $35.00
DOI: 10.1016/S0091-679X(08)00612-2

E. Additional Single-Molecule Information Extracted by FPALM
F. Future Directions
VI. Summary
References

Abstract

Biological imaging has been limited by the finite resolution of light microscopy. Recent developments in ultra-high-resolution microscopy methods, many of which are based on fluorescence, are breaking the diffraction barrier; it is becoming possible to image intracellular protein distributions with resolution of tens of nanometers or better. Fluorescence photoactivation localization microscopy (FPALM) is an example of such an ultra-high-resolution method which can image living or fixed cells with demonstrated lateral resolution of ~34 nm. A detailed description of the methods involved in FPALM imaging of biological samples is presented here, accompanied by comparison with existing methods from the literature.

I. Introduction

The image of a point source has finite size r_0, even if the source is infinitesimal. Therefore, distinguishing multiple point sources from one another is possible when those point sources are separated by more than r_0, but increasingly more difficult when sources are numerous and separated by much less than r_0. In most biological samples, it is advantageous to image large numbers of molecules of interest, and in most cases these molecules are observed within a region containing even larger numbers of water molecules, ions, proteins, nucleic acids, and lipids. Simultaneous resolution of all of these molecules from one another becomes virtually impossible. Thus, resolution limits the size of structures that can be imaged using light microscopy to sizes of order r_0. In wide-field microscopy, the resolution has been quantified by the Rayleigh criterion (Born and Wolf, 1997):

$$r_0 = 0.61\lambda/\mathrm{NA} \quad (1)$$

where λ is the wavelength of the detected photons and NA is the numerical aperture of the lens system.

In laser-scanning microscopes, the resolution is directly related to the properties of the observation volume O(r), the region in which fluorescence is both excited and detected, defined as $\mathrm{O(r)} = \mathrm{I}(r) \cdot \mathrm{C(r)}$, where I(r) is the illumination point-spread function, and C(r) is the detection profile. I(r) depends on the laser illumination wavelength, objective NA, the laser profile in the objective back aperture, objective aberrations, fluorescence saturation effects, and a number of other variables (Pawley, 1995; Sandison and Webb, 1994; Sandison *et al.*, 1995). Illumination

by high-NA lenses can produce a diffraction-limited illumination volume with full width at half maximum (FWHM) of $\sim 0.55\lambda/\mathrm{NA}$ (Pawley, 1995). In confocal microscopy, epifluorescence detection using the same high-NA lens as for illumination and a detector aperture placed in the image plane result in significant improvement in the resolution, but the detector aperture also reduces the fraction of light collected. For an infinitesimal detector aperture, the collection point spread function approaches that of the diffraction-limited illumination profile in the case of an overfilled back aperture (i.e., the $1/e^2$ radius of the laser beam is larger than the radius of the back aperture of the objective lens) and incoherent (uncorrelated) emission (Hess and Webb, 2002; Sandison and Webb, 1994; Sandison *et al.*, 1995) and the resolution can be improved by as much as a factor of $\sqrt{2}$, neglecting the Stokes' shift of the fluorescence relative to the excitation wavelength, distortion of the illumination profile by polarization effects, and lens aberrations. However, the resolution is still limited to some fraction of a wavelength.

Two-photon microscopy provides numerous advantages for imaging biological samples, including reduced out-of-plane photobleaching, excitation of multiple fluorescent probes using the same illumination wavelength, and excellent signal-to-background ratio (Denk *et al.*, 1990; Xu *et al.*, 1996). However, because of the longer wavelengths used to excite fluorescence, and despite the intensity-squared dependence of the excitation rate, in practice the resolution is similar to that of a confocal microscope with detector aperture size optimized for maximum signal-to-noise ratio. Thus, a number of standard far-field methods are limited in resolution to approximately $\lambda/2n$, where n is the refractive index of the medium (Hell, 2007).

One method for resolution enhancement is to extract information about the structure of the object using the "near-field" electromagnetic waves found at distances less than λ from the object. Near-field optics often use an aperture or optical fiber with diameter significantly smaller than λ to create an excitation volume which has a width much less than λ near the aperture. Because coupling the emitted light back through the tiny aperture or fiber tip is often inefficient, a standard objective lens is often used to collect fluorescence excited from single molecules in such applications. The tip can be scanned to image an area with resolution of at least 12 nm under visible illumination (Betzig and Trautman, 1992; Betzig *et al.*, 1991), or better than $\lambda/40$. Near-field interactions between a sharp probe and sample can be used to image at even higher ($\sim$12 nm) resolution (Betzig and Trautman, 1992). However, the requirement for proximity between the probe tip and the sample does pose a significant limitation for many biological applications (Hell, 2007).

Electron microscopy offers tremendous (near-atomic) resolution and has been used extensively to image a variety of biological samples. Unfortunately, requirements for sample fixation, freezing, or other preparation methods, the addition of heavy metals to improve contrast, and the reduced ambient pressure or vacuum for electron beam propagation have so far prohibited successful imaging of living biological specimens. Since understanding dynamics is crucial to the understanding

of biological processes, improved noninvasive methods based on far-field visible-light optics promise to reveal a great deal about biological function.

Development of "super-resolution" methods, namely, techniques that break the diffraction barrier and image samples at length scales much less than a wavelength, is currently of great interest. These methods can be grouped into several categories and compared to highlight advantages and disadvantages.

A. Observation Volume Confinement

The diffraction barrier has been broken using stimulated emission depletion (STED) fluorescence microscopy (Hell and Wichmann, 1994; Klar *et al*., 2000). STED causes molecules excited at the edges of a normal diffraction-limited volume to be driven to the ground state without fluorescence by illuminating them with an annular beam at a frequency that causes stimulated emission from the excited state. Only those molecules at the null (center) of the donut-shaped STED beam remain in the excited state long enough to fluoresce, resulting in emission from a highly confined volume. Focal plane resolution of 15–20 nm has been achieved in fixed biological samples using STED with nonlinear deconvolution (Donnert *et al*., 2006). The concept of STED has been generalized to other reversible saturable optical fluorescence transition (RESOLFT) (Hell *et al*., 2003) techniques, which exploit optically driven transitions between states with drastically different emission properties, such as photoswitching of fluorescent proteins (Hofmann *et al*., 2005) to achieve subdiffraction-limited resolution.

B. Modulated Illumination

4Pi microscopy (Schrader and Hell, 1996) and I^5M (Gustafsson *et al*., 1999) both use two opposing objective lenses to illuminate a sample and collect fluorescence with improved axial resolution. Structured illumination (Gustafsson *et al*., 1999) and saturated structured illumination microscopy (SSIM) use a spatially modulated sample illumination profile to, upon deconvolution, extract information at higher spatial frequencies and thereby improve resolution. SSIM resolution is in principle limited only by signal-to-noise ratio and the photobleaching properties of the probes, with demonstrated resolution of better than 50 nm (Gustafsson, 2005).

C. Hyperlens Imaging

A recent example of hyperlens imaging uses a multilayered anisotropic material with hyperbolic dispersion to convert scattered nonpropagating evanescent electromagnetic waves containing high spatial frequency information about a sample smaller than λ, into propagating far-field electromagnetic waves that were imaged using a high-NA objective (Liu *et al*., 2007). However, such methods have not yet been demonstrated on biological samples.

D. Single-Molecule Localization and Reconstruction

Single-molecule localization and image reconstruction is the basis for several super-resolution methods. Localization, namely, determination of the position of an object using its image, has been achieved with precision as high as 1.5 nm (Yildiz *et al.*, 2003) for the diffraction-limited image of a single fluorescent molecule. Single-molecule detection methods provide additional information about absolute numbers of molecules, motion, and brightness of individual molecules, which can reveal population heterogeneities inaccessible to methods that image an ensemble of molecules. Ultrahigh-resolution colocalization (UHRC) (Lacoste *et al.*, 2000) is a scanning confocal microscopy technique capable of localizing multiple fluorophores that are excitable with a single laser source and of differing emission properties. While UHRC allows for simultaneous imaging of multiple probes, it is still difficult to use to resolve identical probe molecules separated by less than r_0. Fluorescence intermittency has been used to localize single-molecules and single-quantum dots with a precision on the order of tens of nanometers (Lagerholm *et al.*, 2006; Lidke *et al.*, 2005), as well as quantify velocities of individual biomolecules and protein assemblies by fluorescent speckle microscopy (Ponti *et al.*, 2005; Salmon *et al.*, 2002; Waterman-Storer *et al.*, 1998). Single-particle localization in three dimensions has been achieved with $\sim$20 nm resolution and $\sim$30 ms time resolution (Levi *et al.*, 2005a, b). Other methods have exploited the photobleaching characteristics of fluorophores to localize single molecules. Single-molecule high-resolution imaging with photobleaching (SHRImP) (Gordon *et al.*, 2004) and nanometer-localized multiple single-molecule (NALMS) fluorescent microscopy (Qu *et al.*, 2004) both take advantage of the stepwise photobleaching of single molecules to localize their positions with precision on the order of a few nanometers. So far, such photobleaching methods have required that relatively few fluorophores reside within a cross-sectional area of radius r_0. The points accumulation for imaging in nanoscale topography (PAINT) (Sharonov and Hochstrasser, 2006) method localizes single molecules that fluoresce as they bind to a target object of interest and then photobleach. While the methods described above provide a means of subdiffraction localization-based resolution, control over the density of fluorescent molecules in the field of view requires adjustment of the concentration of fluorophores.

Techniques such as fluorescence photoactivation localization microscopy (FPALM) (Hess *et al.*, 2006), and photoactivated localization microscopy (PALM) (Betzig *et al.*, 2006), which use photoactivatable fluorescent proteins (PA-FPs) or other photoactivatable fluorophores, allow for direct *optical* control over the number of fluorescent molecules by adjusting the rates of photoactivation and photobleaching (Fig. 1). In a similar manner, stochastic optical reconstruction microscopy (STORM) (Rust *et al.*, 2006) uses photoswitchable combinations of organic fluorophores to control the number of molecules fluorescing at a given time. Images are then reconstructed from the coordinates and intensities of localized molecules.

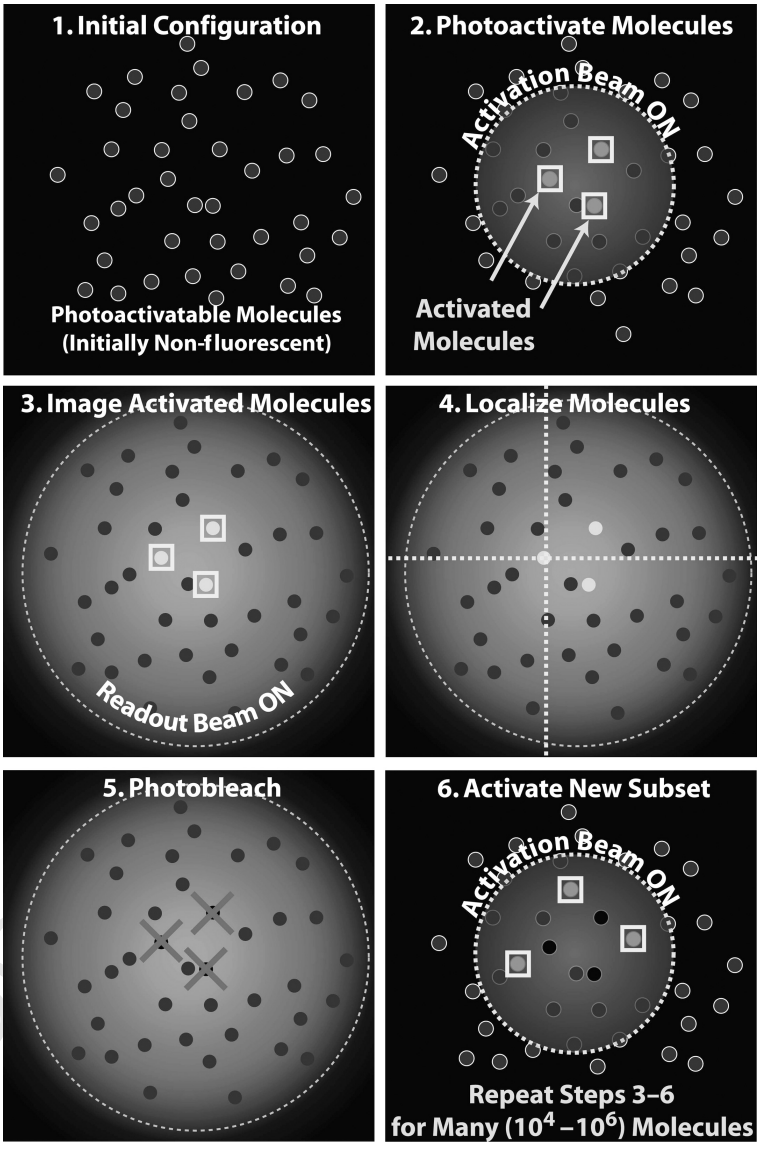

Fig. 1 Principle of fluorescence photoactivation localization microscopy (FPALM). (1) Initially, all molecules in the sample are inactive (dark circles), namely, in a nonfluorescent state, and virtually no fluorescence is emitted from the sample. Two lasers are used to control the number of active (potentially fluorescent) molecules. (2) A high-energy visible (typically ~400 nm) laser, called the activation laser (smaller dashed circle), is used to activate a small number of molecules in the sample (boxes). This number is kept small by making the activation laser intensity sufficiently weak in the focal plane of the sample. Activation of molecules occurs randomly: the probability of activation of a given molecule is proportional to the intensity of the activation laser at the location of that molecule, but typically very small. (3) The activation laser is turned off and molecules that were activated are read out, using

Compared to confined and modulated illumination methods, FPALM can be used in a standard wide-field microscope, does not require ultra-fast pulsed lasers or image deconvolution, and does not rely on nonlinear excitation. Compared to other single-molecule localization techniques, FPALM, PALM, and STORM also have the advantage that they rely on photophysical properties to control the number of fluorescent molecules in the field of view. The flexibility of using genetically encoded fluorescent markers such as green fluorescent proteins (GFPs) is both powerful and efficient, allowing existing GFP-constructs to be converted into PA versions using standard molecular biology procedures.

II. Theory and Rationale

The basis of FPALM (Fig. 1) is the localization of large numbers of single fluorescent molecules, imaged in small numbers at a time. Localization is defined as determination of the two- or three-dimensional position of the emitting object. In contrast, resolution is defined as determination that two emitting objects are distinct from one another. In FPALM, large numbers of molecules are ultimately localized within an observation area, but for those molecules to be resolvable from one another, a small number must be fluorescent at a given time. Thus, control over the number of fluorescent molecules visible at a given time is crucial. This control is achieved by the use of probes which can be optically switched from an inactive (nonfluorescent) state (I) into an active (potentially fluorescent) state (A). Irreversible or reversible activation can be used as long as the number of fluorescent molecules can be controlled within the observation area. The transition between inactive and active states is typically achieved by an activation laser, but a lamp or light-emitting diode (LED) could in principle be used as long as sufficient intensity is obtained at the sample. The activation laser is typically a different (higher) frequency than the readout laser used to image and photobleach the active molecules. The activation laser is used to stochastically activate a small number of inactive molecules, which are then imaged under excitation by the readout laser until they stochastically photobleach (or become deactivated in the case of reversible activation). The number of active molecules must be kept small enough

a second, typically lower energy laser, called the readout laser. Readout means detection of fluorescence from activated molecules (gray circles) within the illuminated area. During the time that the readout laser is on (and typically during the entire process), a high-sensitivity charge coupled device (CCD) camera is recording a movie of the same field of view being illuminated. (4) The movie frames are analyzed to identify and localize activated molecules (dashed lines delineate coordinates of active molecules) for as long as they remain fluorescent. (5) Molecules spontaneously photobleach (crosses) under the high-intensity illumination of the readout beam, eventually reducing the number of visible molecules significantly. (6) A new set of molecules is activated by again briefly turning on the activation beam (equivalent to step 2). Steps 3–6 are repeated many times, either until enough molecules have been activated and imaged to obtain the desired image quality, or until all photoactivatable (PA) molecules within the sample have been exhausted.

(by adjusting the intensity of the activation laser) that virtually all molecules are optically distinguishable. Quantitatively, this requires that the average separation between molecules $L_0 \gg r_0$ (typically $L_0 > 4r_0$), where r_0 is the diffraction-limited resolution given by Eq. (1). Molecules closer than this minimum are excluded from analysis because of the difficulties in determining their positions accurately. The process of activation, imaging, and photobleaching is repeated until the molecules in the sample are exhausted, or until sufficient numbers of molecules have been imaged for the particular application. Figure 2 shows examples of the actual readout and activation laser beam profiles, images of single molecules identified by the algorithm, and plotted positions of molecules without and with intensity weighting.

In practice, the sample is placed on the stage of a microscope, near the focus of a high-NA objective lens (Fig. 3). Only molecules within the focal plane can be successfully imaged and localized. During acquisition, the sample sits under

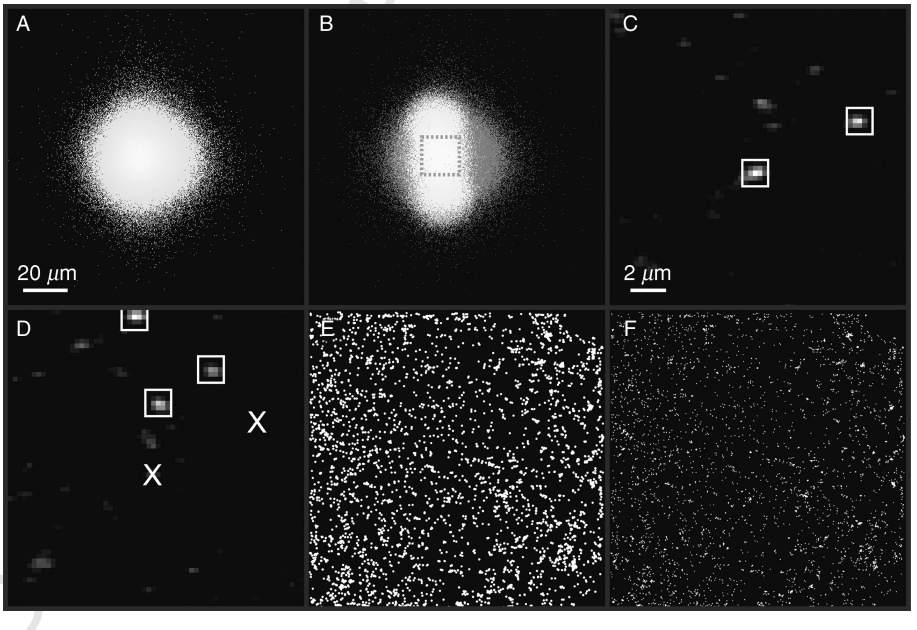

Fig. 2 Fluorescence photoactivation localization microscopy (FPALM) method illustrated using experimental results. (A) Profile of readout beam (488 nm). (B) Merged profiles of readout and (noncircular) activation (405 nm) beams. Dark gray indicates regions illuminated by the readout beam, while white indicates regions illuminated by *both* the readout and activation beams. (C–F) Examples of molecules imaged within the boxed region in (B). (C–D) Two successive frames from a time series acquisition of caged-fluorescein imaged on a coverslip. White boxes indicate localized single molecules in the given frame. An "*X*" in (D) indicates locations of molecules that were identified in the previous frame (C) but presumably photobleached during or before the acquisition of the frame shown in (D). (E) Rendering of positions of all 3,850 molecules localized over the entire acquisition (all molecules shown with same intensity and size). (F) Rendering of positions of all localized molecules, plotted with intensity proportional to the number of detected photons.

continuous illumination by the readout beam and continuous imaging using a high-sensitivity charge coupled device (CCD) camera which is sensitive enough to detect single fluorescent molecules. Pulses of the activation laser are applied whenever necessary to increase the number of active molecules in the observation area.

Once molecules have been activated, imaged, and photobleached, analysis of the images is performed to determine the positions of the molecules by localization. The precision with which a fluorescent object can be localized in two dimensions is given by σ_{xy}, where

$$\sigma_{xy}^2 = \frac{r_0^2 + q^2/12}{N} + \frac{8\pi r_0^4 b^2}{q^2 N^2} \tag{2}$$

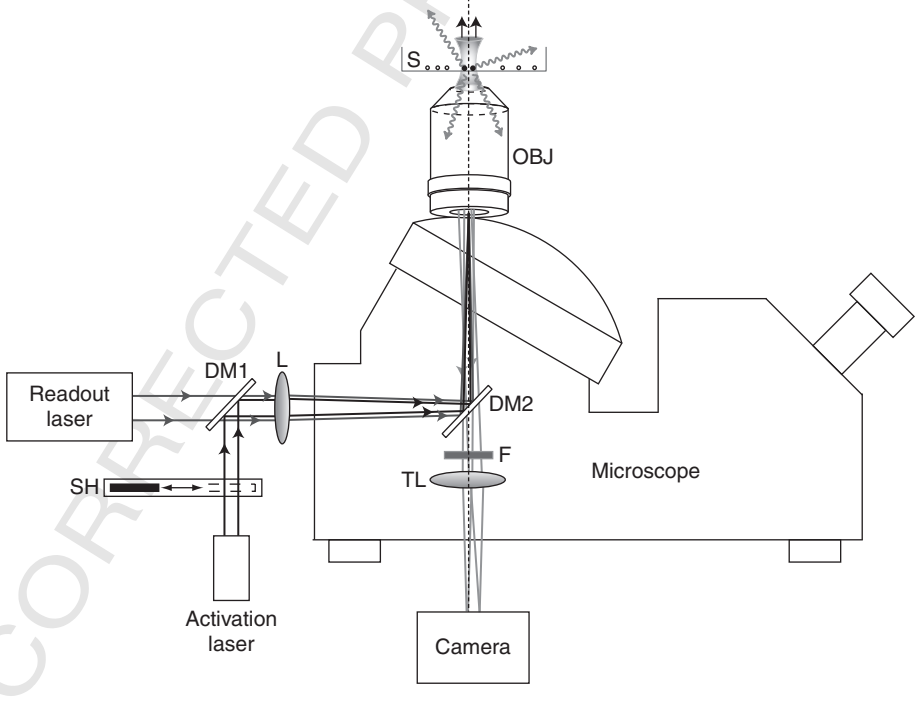

Fig. 3 The experimental geometry of fluorescence photoactivation localization microscopy (FPALM) is based on a wide-field fluorescence microscope with a high-sensitivity camera for single-molecule imaging. The activation laser beam is reflected by a dichroic mirror (DM1) and becomes collinear with the readout laser beam (passed by DM1). Both beams are focused by a lens (L) and reflected by a second DM2 to form a focus in the back aperture of a high numerical aperture objective (OBJ), which causes a large area of the sample (S) to be illuminated. Some emitted fluorescence photons (gray wavy arrows) are collected by the same OBJ, pass through DM2 and an emission filter (F), and are focused by the microscope tube lens (TL) to form an image on the camera. A shutter (SH) controls the activation laser beam for intermittent illumination. For simplicity, various mirrors for steering the laser beams, neutral density filters for attenuating the lasers, and the microscope stage and condenser are not shown. Drawing is not to scale.

where r_0 is the standard deviation of the point spread function, N is the total number of photons collected (not photons per pixel), q is the size of an image pixel, and b is the background *noise* per pixel (not background intensity). From Eq. (2), it is clearly possible to localize single fluorescent molecules with significantly better precision than $\pm r_0$. Thus, if a large number of molecules can be individually localized, their positions and intensities can be used to produce a map (image) of the distribution of molecules with localization-based resolution given by Eq. (2). In addition, the number of localized molecules must be large enough to represent the various regions within the observation area; a single molecule localized to ± 1 nm does not constitute an ''image'' of the sample at 1-nm resolution.

The localization precision σ_{xy} can be improved by increasing the number of detected photons. Probes which emit large numbers of photons before photobleaching are therefore advantageous. Many intrinsically fluorescent proteins (including GFP and dsRed) have (irreversible) photobleaching quantum yields Φ_B between 10^{-4} and 10^{-6} (Dickson *et al.*, 1997; Heikal *et al.*, 2000; Hess *et al.*, 2004; Moerner *et al.*, 1999), where the value of Φ_B is the probability per excitation that the fluorophore is converted into a (permanently) non-fluorescent form. The ratio Φ_{Fl}/Φ_B gives a measure of the average number of photons emitted by a fluorophore before photobleaching, where Φ_{Fl} is the fluorescence emission quantum yield, and should be maximized by choice of fluorophore whenever possible. Including the detection efficiency Φ_{det}, the number of detected photons $N_{det} = \Phi_{Fl}.\Phi_{det}/\Phi_B$ yields a localization precision

$$\sigma_{xy}^2 = \frac{r_0^2 + q^2/12}{N_{det}} + \frac{8\pi r_0^4 b^2}{q^2 N_{det}^2} = \frac{\Phi_B(r_0^2+q^2/12)}{\Phi_{det}\Phi_{Fl}} + \frac{8\pi r_0^4 b^2 \Phi_B^2}{q^2 \Phi_{det}^2 \Phi_{Fl}^2} \quad (3)$$

III. Methods

A. Choice of Probe

The choice of an appropriate probe is dependent on its photophysical properties. Probes with high photoactivation yields and low rates of spontaneous activation (relative to light-induced activation) are desirable for controlling the number of active molecules. Unfortunately, there is currently very little data available on activation yields. For a recent review of PA and photoswitchable proteins see Lukyanov *et al.*, 2005. Probes should also have large contrast ratios; that is to say that the fluorescence from the inactive state must be weak in comparison to the active state since fluorescence from the inactive state contributes to the background noise (Hess *et al.*, 2006).

Maximizing localization-based resolution demands maximizing the number of collected photons, which implies that probes with high fluorescence emission rates and large numbers of photons emitted before photobleaching are attractive candidates for FPALM applications. While a large photobleaching quantum yield

ultimately results in fewer total emitted photons, a finite photobleaching yield is necessary to prevent the accumulation of too many active molecules, making localization impossible. More specifically, to control the number of active molecules requires that under imaging conditions the photobleaching rate (plus the deactivation rate in the case of reversible activation) must be greater than or equal to the activation rate (Hess *et al.*, 2006). If multiple probes are to be used, consideration must be taken to ensure that the emission of each probe will be spectrally separable using appropriate filter combinations.

B. Choice of Filters

The choice of appropriate filters is determined by the probes and the lasers being used to excite those probes. A suitable dichroic mirror must be chosen that can sufficiently reflect both the readout and activation beams while maximizing transmission of the desired fluorescence. Emission filters should be chosen to further reduce scattered laser light and other background while selectively transmitting as much of the probes emission spectra as reasonable. The use of multiple probes will require additional dichroic mirrors and emission filters to separate the emission and minimize cross talk between channels.

C. Alignment and Characterization of the Illumination Area

FPALM requires the collinear alignment of a readout laser beam and a (typically shorter wavelength) activation laser beam. These beams are then focused to a small spot at the center of the back aperture of the microscope objective lens to produce an illumination area at the sample which is large enough to encompass the desired region of interest (ROI), such as an entire cell. If a long-pass (only wavelengths greater than a certain cutoff wavelength are transmitted) dichroic mirror is used to merge the two beams, alignment is most efficiently achieved by first aligning the straight-in (parallel) beam (typically the readout laser) into the center of the field of view, without the lens in place. The lens, typically mounted near or just inside one of the input ports of the microscope, should then be aligned to focus the readout beam at the center of the objective back aperture (the opening where the laser enters the objective). The profile of the expanded beam area can then be viewed via the display of a CCD camera by focusing into a dilute solution of an appropriate fluorophore. This solution should be dilute enough so as not to saturate the camera, and the emission range of the fluorophore should be chosen to be compatible with the filter sets being used. Collinear alignment of the activation laser beam is now easily accomplished by adjusting the dichroic mirror while monitoring the camera view. Alignment of the centers of both beams is recommended. However, while the beam centers should be aligned as closely as reasonably achievable, as long as the two profiles are overlapping it will be possible to control the number

of active molecules within the area illuminated by both the activation and readout beams. Images of the profile of both beams should now be obtained for later reference. Example beam profiles are shown in Fig. 2. The activation beam area may be smaller than the readout beam to maximize activation intensity. The readout beam may be spread over an area larger than the desired ROI to yield a nearly uniform illumination intensity within the ROI.

Generally, illumination by the activation source will be intermittent, as is required to maintain a small number of (from ten to a few hundred) visible molecules within the ROI. Activation pulse duration is ideally regulated electronically (e.g., by computer) to allow a well-defined timing protocol or synchronization with various events such as camera frames, but it is also possible to manually control activation. It is also convenient to have shutter control over the readout source. In cases where having an expanded illumination area results in insufficient activation intensity (due to spreading the laser power over too large an area), it may be necessary to rotate the lens near the back port of the microscope out of the beam path in coordination with the activation pulse (e.g., by having the lens mounted in a motorized filter wheel) to produce a more intense (although smaller) activation area.

In some cases, a PA probe will be inefficiently activated by the readout beam. For some fluorophores, this readout-induced activation rate will be so low under normal readout laser intensities that it is negligible compared to the rate induced by the activation beam. For other molecules, the readout-induced rate will be so large that it prohibits FPALM because the activation cannot be efficiently controlled, and too many molecules become visible in the illuminated area. However, if the readout-induced rate of activation is comparable to the rate of activation induced by the activation beam itself, the activation beam is essentially redundant and can be omitted from the setup. In fact, for PA-GFP activated at 405 nm and imaged (readout) at 496 nm, the readout-induced activation rate is high enough to allow readout of thousands of molecules without illuminating the sample at 405 nm. The relative rates of readout-induced and normal activation can be adjusted to make the activation by a 1-s exposure of 405 nm light with $\sim$0.1 mW at the sample comparable to the activation during $\sim$10 s of continuous illumination at 496 nm with $\sim$10 mW at the sample (M. Gunewardene, *unpublished results*). Such an FPALM setup is even simpler to align and requires only that the readout beam be turned on as image acquisition with the camera begins. One limitation to this version of the method is that fluorophores with an advantageous readout-induced activation rate must be used. Furthermore, if the number of molecules in the sample is too high initially, the activation during readout illumination will lead to too many molecules becoming active in the early stages of the acquisition, preventing their positions from being determined. In such a case, one must wait until after significant photobleaching occurs to reduce the total number of molecules available to be localized, to allow the individual molecules to be separated clearly.

D. Choice of Sample Region

Transmitted light from a microscope lamp can be used to locate cells or other sample features for imaging. To reduce unintentional activation of the sample before imaging, lamp light should be long-pass filtered to remove as much intensity as possible from within the range of activation wavelengths (e.g., $\lambda <$ 500 nm in the case of PA-GFP). For imaging, the sample should be positioned within the region of overlap between readout and activation beams. Manually marking the boundaries of both beam profiles on the display can be helpful. Sample regions should be selected for imaging when single molecules can be observed by eye or with the camera (usually with stepwise blinking and/or bleaching) during illumination with the readout source. Numerous fluorescent molecules may be present during initial illumination due to any molecules activated before the start of the acquisition (e.g., by inadvertent exposure to room light or ultraviolet sterilization lamps inside the cell incubator). When too many molecules are emitting at once, single molecules will not be distinguishable by eye and it will be necessary to allow some of these molecules to photobleach before beginning an acquisition. To localize an efficient number of activated molecules, it is desirable to have active molecules separated by $\sim 4r_0$ on average (Hess *et al.*, 2006). For PA-GFP imaged by a 1.2 NA objective ($r_0 \sim 260$ nm), the optimal density would be $\sim$3 activated molecules per 10 μm^2 area. Once any inadvertently activated molecules have sufficiently photobleached, the density of activated (fluorescent) molecules can be controlled with intermittent pulses of the activation beam and a suitable continuous intensity of the readout beam. In short, an acquisition generally consists of continuous illumination by the readout beam and short pulses ($\sim$1 s) of the activation beam administered whenever the number of visible molecules is fewer than $\sim 0.1/\mu$m^2.

During sample region selection (before beginning the acquisition), it is also necessary to determine the location of the focal plane within the sample. Viewing with transmitted light may be of assistance in locating features on a surface, but this method is only sensitive to gross movements ($>>1$ μm) in the axial direction. For applications involving three-dimensional samples such as cells, a priori knowledge of the features or labeling with a secondary fluorescent marker (of distinguishable emission) may be necessary to identify the focal plane. For example, when imaging membrane-bound proteins in a cell, the coverslip-proximal membrane can be located by focusing below the coverslip and then moving the focus upwards through the sample until fluorescent molecules first come into focus. If imaging structures within the cell, the use of a secondary marker with emission distinct from the FPALM probe can serve as a reference.

Frame acquisition (exposure) times and overall acquisition length (total number of frames) vary based on the photophysical properties of the fluorophore used and the required resolution. The lower limit on frame acquisition time is determined by the detected photon rate per molecule such that a sufficient number of photons are detected per frame to obtain the desired resolution. In samples with immobile

molecules (e.g., fixed cells or molecules immobilized on a surface), the average photobleaching time should also be adjusted via the intensity of the readout laser to be approximately equal to the frame acquisition time. Times in the range of 100–150 ms are generally sufficient to yield a demonstrated resolution of ~30 nm using PA-GFP in cells illuminated at ~100–200 W/cm^2. In live cells where labeled molecules may undergo diffusion, the acquisition time should be short enough such that the image of a single molecule does not experience additional blurring due to diffusion. Motions of molecules can be quantified if the photobleaching time is at least twice the frame acquisition time (see also section on live-cell imaging).

E. Position Stability

Because localization of molecules can be achieved with nanometer precision, position stability of the sample relative to the imaging system is crucial. A nonmotorized microscope mounted on a vibration isolation table in a basement room provides reasonable position stability over timescales of minutes. Microscope lateral stability can be characterized by time-lapse transmitted light imaging of 1-μm diameter polystyrene spheres. Spheres are dried on a coverslip at low density, and imaged at ~8 frames per second under lamp illumination for 20.6 min. Images of the spheres are then analyzed to determine the X-Y (lateral) coordinates of the sphere as a function of time. A histogram of the positions (after subtraction of the mean position) of a single sphere is shown in Fig. 4 along with corresponding fits using a Gaussian. Twice the standard deviation of the Gaussian yielded $2\sigma_X =$ 7.1 nm and $2\sigma_Y = 5.9$ nm after 20.6 min. Thus, for acquisitions of roughly 20 min or less, localization precision, not drift, will dominate the resolution of images obtained if localization precision is >7 nm, as is typical in live cells and many other applications.

Longer acquisitions may be desirable and will require further attention to sample drift. In addition to the necessary characterization of microscope stage drift, positions of molecules may also be corrected by the use of fiduciary marks, such as quantum dots which are bright and photobleaching-resistant, or fluorescent microspheres which carry large numbers of fluorophores (Betzig *et al.*, 2006). While for shorter acquisitions, the necessary maintenance of the position of the focal plane can be achieved manually, longer acquisitions may benefit from automatic focus correction. Axial motion of much less than the depth of field ($<< \pm 1$ μm) over the experimental timescale may be acceptable if a two-dimensional sample image is desired, and the sample is approximately planar. However, samples which have significant three-dimensional extent may be difficult to image if fluorescent molecules are present in many focal planes, as activation can occur above and below the focal plane, and may eventually make identification of the original (desired) focal plane difficult.

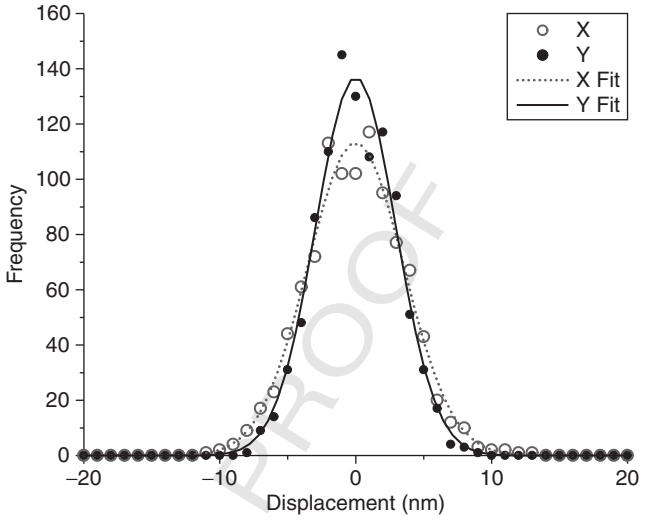

Fig. 4 Quantification of microscope stability by repeated imaging of single immobilized bead. Polystyrene spheres with 1-μm diameter were imaged repeatedly under transmitted light illumination, and then their positions were quantified as a function of time for 20.6 min. Twice the standard deviation in the lateral positions $2\sigma_X = 7.1$ nm and $2\sigma_Y = 5.9$ nm provides a measure of lateral position stability over relevant experimental acquisition timescales. The measured distribution of positions was fitted with a Gaussian in X and Y (curves labeled X Fit and Y Fit, respectively).

F. Fluorescence Background

Before acquiring data, experimental considerations should always be taken to minimize background light from reaching the camera(s). Using lens tubes to shield the image beam path from the microscope to the camera is useful in eliminating background signal generated from external sources. Common internal sources of background include fluorescence from inactive molecules, out-of-focus active molecules, the immersion liquid, a dirty or dye-contaminated objective lens, the coverslip (fused quartz is sometimes better than glass), and scattered laser light. Cell imaging inevitably results in additional sources of background including autofluorescence, and fluorescence from the media (including ingredients such as phenol red and serum) and residual transfection reagents. The appropriate choice of filters will also help reduce background signal.

Before the position of a single molecule can be determined, a background subtraction is typically performed (background counts do not in general help to determine the position of an object, and add artificially to the apparent brightness of molecules and required threshold levels). First, the zero level (the counts measured with the camera on but no light striking its surface) should be subtracted from all images before any analysis is performed. Background subtraction methods include (a) constant baseline (uniform) or (b) position-dependent (nonuniform).

In the uniform method, a single (potentially time-dependent) value is subtracted from all pixels within the image. Typically, this value is chosen as the average pixel value from a region in the image where there is no fluorescence, or is chosen from analysis of the image intensity histogram.

For cell imaging, due to background fluorescence from inactive or out-of-focus active molecules, a nonuniform background subtraction is sometimes more appropriate. A typical method for nonuniform background subtraction is to generate a time-averaged wide-field image from all frames in the acquisition. From each individual frame to be analyzed, the average wide-field image is subtracted, weighted by (typically 95% of) the average intensity of that given frame. Such a subtraction requires the illumination profile within the ROI to be as uniform as possible, so that photobleaching occurs at a similar rate across the area.

G. Adjustment of Thresholds

The analysis of single-molecule localization begins with sequential analysis of each frame in the time series to identify and determine the position of individual molecules. In practice, custom or prepackaged software is used to select a ROI from a background subtracted image. After background subtraction, each pixel of the ROI is scanned to identify objects with intensity above an identification (ID) threshold usually on the order of a few hundred photons. Each identified object is surrounded by and centered within a square (typically 5×5 pixel) box that must meet additional criteria to ultimately be analyzed as a single molecule. Within this box, a minimum number of (typically 3–5) pixels must exceed a second threshold (typically 50–80% of the ID threshold, depending on the size of the image of the single molecule relative to one pixel) and no more than a certain maximum number of (typically 8–15) pixel values may exceed a third threshold (typically between 50% and 100% of the ID threshold) or this object will be rejected as too dim or too large, respectively, to be a single molecule.

H. Rendering the Results

FPALM images can be rendered by either of two methods: (A) unweighted, point-like plots of the positions of localized molecules, or (B) weighted plots of the positions of localized molecules, plotted as a spot with a Gaussian profile, an intensity proportional to the number of photons detected from each molecule, and a radius equal to the calculated or experimentally determined localization-based resolution. Because the weighted plots take into account the intensity and position uncertainty of each molecule, the resulting image is in some ways a more realistic representation of a fluorescence image with ultra-high resolution. Examples of both are shown in Fig. 2E–F. Typically, all molecules localized within a particular area are rendered simultaneously, but in live cells or other time-dependent samples, time-dependent images may be rendered using subsets of molecules localized during various time periods. A threshold which includes only

molecules within a particular range of intensities, or above a minimum intensity, can also be applied.

I. Biological Applications in Live Cells

Use of FPALM in live cells requires particular diligence for several reasons. In live-cell experiments, the molecules of interest may be themselves moving, and therefore their images will be further blurred compared to the ideal diffraction-limited point spread function. For this reason, the acquisition rate should be fast enough that the displacement of single molecules being localized is much less than the width of the point spread function. If the molecules are diffusing, this implies that $D\tau << r_0^2$ where τ is the frame acquisition time, and D is the diffusion coefficient. For example, hemagglutinin (HA) from influenza is a transmembrane protein with exceptionally slow diffusion; for the Japan variant of HA, using fluorescence photobleaching recovery, the diffusion coefficient is $D_{HA} = 0.069\ \mu m^2/s$ (Shvartsman *et al.*, 2003). Within $\tau = 0.1$ s, each HA will on average move within an area of $0.0069\ \mu m^2$, which is approximately equal to $\sim 83 \times 83$ nm. For an emission wavelength of 520 nm, and a 1.2 NA objective, $r_0 = 264$ nm, and so diffusion of HA molecules will only modestly blur the image during the frame time. In contrast, for a faster-moving protein such as KRas with $D \sim 1.1 \pm 0.3\ \mu m^2/s$ (Kenworthy *et al.*, 2004) and $\tau = 1$ s, the motion covers an area $D\tau = 1.1\ \mu m^2$ which is significantly larger than r_0^2 and the image would be expected to be drastically blurred, making such an acquisition very difficult to analyze. Furthermore, proteins which diffuse in three dimensions may move into or out of the focal plane, causing additional difficulty in analysis of results. Slowly moving plasma membrane-bound proteins are therefore good candidates for FPALM in live cells. Figures 5 and 6 show examples of FPALM images of PA-GFP-tagged influenza HA in fixed fibroblasts. High acquisition frame rates can reduce the motion of molecules within one frame.

IV. Materials

Cells are grown in chambers with a #1.5 coverslip bottom (e.g., Nunc Lab-Tek II growth chambers, #12-565-8 from Fisher Healthcare, Houston, TX) and fixed when necessary. Cells expressing a PA-GFP-tagged protein of interest or other PA-FP are illuminated by 6–10 mW of continuous-wave readout laser power (typically an Argon ion laser at 496 nm for excitation of PA-GFP), spread over an area of $\sim 1000\ \mu m^2$ to yield ~ 600–$1000\ W/cm^2$. For activation, 0.05–1.5 mW of power at 405 nm is used (e.g., the BCL-405 laser from Crystalaser, Reno, NV) which is spread over ~ 125–$250\ \mu m^2$ to yield 20–$1200\ W/cm^2$. As described above (see also Figs. 2 and 3), the activation beam is aligned to illuminate the same

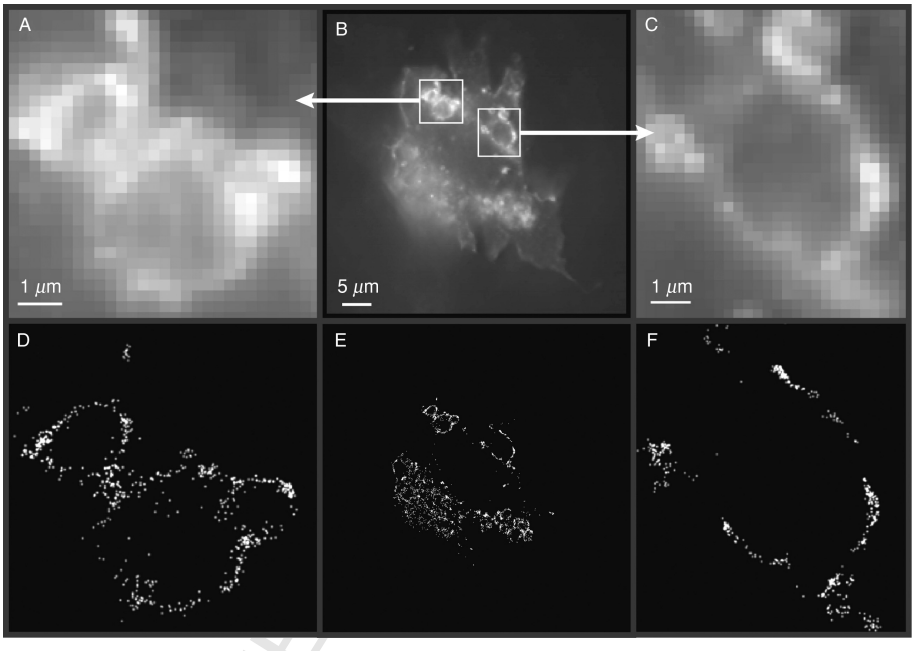

Fig. 5 Wide-field fluorescence (B) and fluorescence photoactivation localization microscopy (FPALM) images (E) of the protein hemagglutinin tagged with photoactivatable-green fluorescent protein (PA-GFP) in a fixed HAb2 fibroblast. (A, C, D, F) Zoom-in of selected regions to show agreement with wide-field fluorescence (A, C) and illustrate improvement in resolution by FPALM (D, F). Note that contrast was adjusted in (E) for visualization. The pairs of images (A and D), (B and E), and (C and F) have the same scale.

(central) region of the field as the readout beam. The readout beam continuously illuminates the sample during data acquisition, while the activation beam is pulsed as needed for ~1–10 s to photoactivate PA-GFP molecules whenever the density of visible molecules within the sample declines to fewer than $\sim 0.1/\mu m^2$. Photoactivated molecules are visualized by imaging the fluorescence onto a CCD camera (Quantifire; Optronics, Goleta, CA) or an electron-multiplication CCD (Cascade 512B; Photometrics, Tucson, AZ, or iXon; Andor Technology, South Windsor, CT). Camera settings include (A) Quantifire: 2×2 binning, 0.1–0.2 s acquisition time, and gain 6–8, and (B) Cascade 512: 1×1 binning, 0.15 s acquisition time, on-chip multiplication gain 1500–2000, and conversion gain 6 e^-/ADU.

Estimated prices for components include inverted fluorescence microscope: $15–25k, high-NA objective lens: $7k, electron-multiplying CCD camera: $25–40k, 405 nm laser for activation: $5–10k, 488 nm laser for readout: $5–15k, miscellaneous optics, mounts, dichroic mirrors, and filters: $8k, computer and Matlab software: $2–3k, computer-controlled shutter: ~$1k.

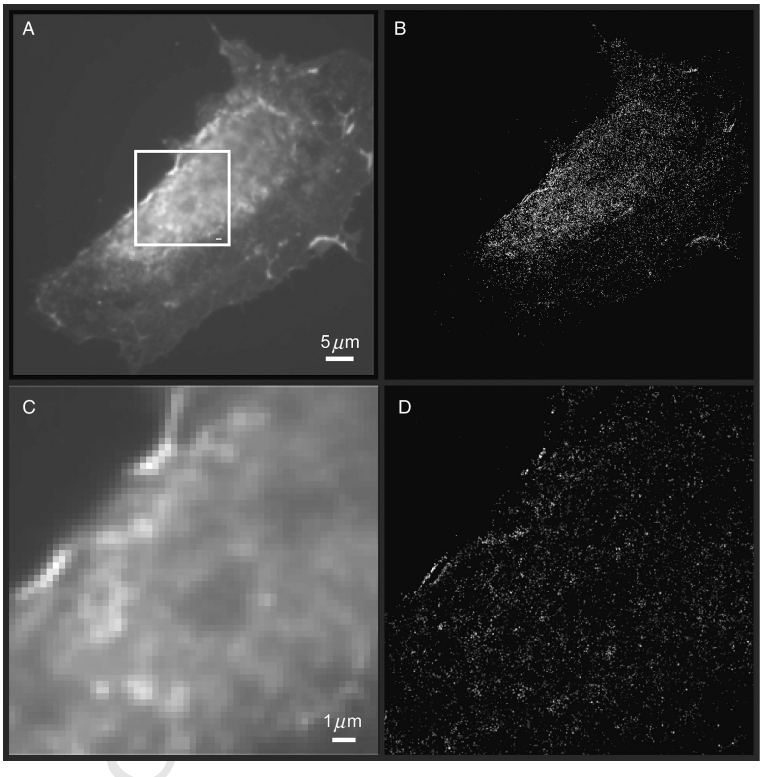

Fig. 6 Wide-field fluorescence (A) and fluorescence photoactivation localization microscopy (FPALM) images (B) of hemagglutinin tagged with photoactivatable-green fluorescent protein (PA-GFP) in a fixed HAb2 fibroblast. Here, a large number of molecules with high brightness have been localized ($n \sim 40{,}000$) in a large cell ($\sim$60 μm in width), so that the molecular coordinates obtained span a wide (more than three orders of magnitude) range of length scales. (C–D) Zoom-in of boxed region showing the improved resolution of FPALM. Note that the contrast was adjusted linearly in (B, D) for visualization.

V. Discussion

Before interpreting FPALM images, it is highly recommended that users image a sample with known geometry to calibrate the microscope and method. While there is no particular sample that serves all purposes, one example of a calibration sample is the annealed R-cut sapphire surface shown in Fig. 7. The surface of this sample, which was described in detail previously (Hess *et al*., 2006) is made up of terraces with straight edges and atomic-scale step sizes. The sample was coated with a drop of PA-GFP in solution, allowed to dry, and imaged using FPALM. The resulting image was compared with atomic force microscope (AFM) images of different regions on the same sample. The width of and spacing between the

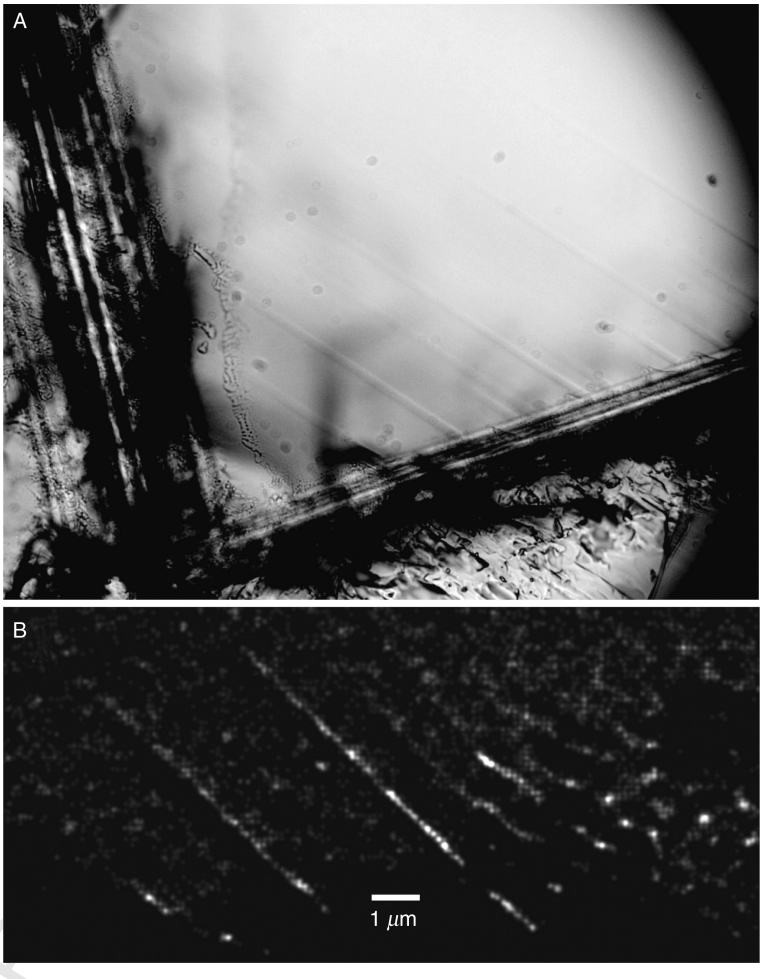

Fig. 7 Fluorescence photoactivation localization microscopy (FPALM) images of atomic terraces on an annealed sapphire surface reveal structures below the diffraction limit of light. A wafer of single-crystal sapphire within 0.05° of R-cut was annealed at 1700 °C in air for ten hours, cooled, cleaned, coated with a thin layer of photoactivatable-green fluorescent protein (PA-GFP), and imaged by wide-field transmitted light (A) and by FPALM (B). The surface contains terraces which appear as straight lines in (A) and (B). The sharp, corner-like edges of the terraces were imaged by atomic force microscopy to have a width of ~70 nm (Hess *et al*. 2006). FPALM results yielded a step width of 73 ± 3 nm defined by the $1/e^2$ width of the image of a single step, or 86 ± 4 nm defined by the full width at half maximum of the same step. These results demonstrate an independent confirmation of the FPALM results and prove that the method can image structures smaller than the diffraction-limited resolution of light, which in this case was ~264 nm. The FPALM image was generated by plotting the positions of all molecules weighted by their intensities and convolving the image of those plotted positions with a Gaussian filter with $1/e^2$ width of 73 nm (a conservative estimate of the resolution). Approximately 6,665 molecules are shown in panel (B).

terraces was found to agree by both methods, confirming that the method could successfully image a sample of known geometry with ~86 ± 4 nm resolution or better, more than threefold better than the diffraction-limited resolution of 264 nm for the same setup. Figure 8 shows a coverslip scored with a crisscross pattern of scratches, labeled with PA-GFP, and imaged by FPALM. Small features which

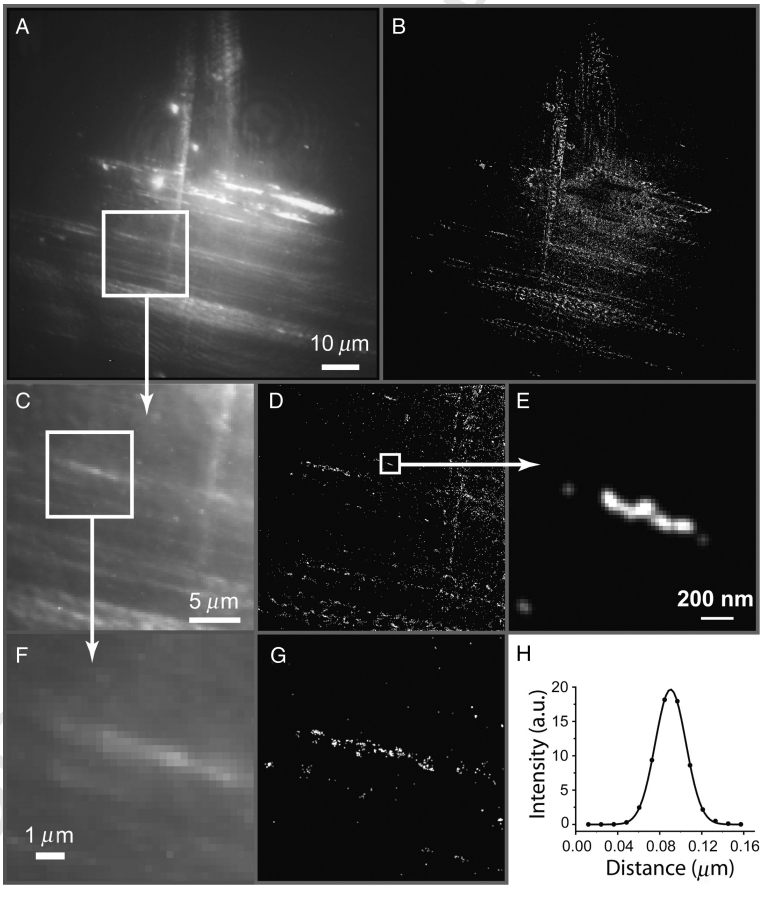

Fig. 8 (A) Wide-field fluorescence and (B) fluorescence photoactivation localization microscopy (FPALM) images of photoactivatable-green fluorescent protein (PA-GFP) in solution dried on a scratched coverslip. Two sets of approximately perpendicular scratches were formed by dragging a razor blade twice across the surface. (C–D) Zoom-in of boxed region in (A) showing (C) wide-field fluorescence and (D) FPALM images. Zoom-in of boxed region in (C) showing (F) wide-field fluorescence and (G) FPALM images. Note the significant improvement in resolution using FPALM. (E) Zoom-in of boxed region in (D) demonstrating the subdiffraction resolution of FPALM. Note that the contrast was adjusted linearly in (B, D, G) for visualization. (H) The cross-section of a linear structure within the same image was fitted with a Gaussian, yielding a full width at half maximum of ~34 nm and a $1/e^2$ radius of ~29 nm, demonstrating nearly eightfold improvement in the resolution compared to wide-field fluorescence microscopy.

collected the PA-GFP are visible with dimensions as small as ~34 nm in full width at half maximum, nearly eightfold smaller than the diffraction-limited resolution.

A. Density of Localized Molecules

If the goal is to reliably image structures at a resolution below the diffraction limit, the density of molecules within the structure of interest is arguably as important as the precision with which those molecules are localized. Too low a density of molecules (too high a sparseness) within a structure leads to large uncertainties in the concentration of molecules; for molecules distributed at a given density within a small region, following Poisson statistics the uncertainty σ_N in the number of molecules N, will be equal to $N^{1/2}$. Thus, even if the molecules are localized with phenomenal precision (e.g., $<<1$ nm), the resulting image will have an uncertainty in the density which is quite large if the number of molecules within a given area is small (e.g., <10). The effect of having a low number of molecules on FPALM images obtained with satisfactory localization precision is illustrated in Fig. 9. Even a sharp edge can be difficult to discern if the density of molecules is too small (Fig. 9A). In practice, localized molecules will have a distribution of intensities; those with the highest intensities will in general be fewer than the majority with average intensity. Thus, there will be a trade-off between generating an image with very many molecules (reduced sparseness) and an image which includes the molecules with the most precisely defined positions (those with the highest intensities).

B. Factors Which Can Bias the Measured Distribution of Molecules

To obtain an FPALM image which accurately reflects the real distribution of molecules in the sample, one must consider the same factors which can bias the image in a normal fluorescence microscope, nonuniform illumination, background and out-of-focus fluorescence, time dependence of the sample, optical aberrations, vibrations, and other motions of the sample relative to the microscope during acquisition. However, several additional effects can bias the measured distribution of molecules in an FPALM microscope. Because FPALM relies on identification and localization of single molecules, if the density of fluorescent molecules gets so high that individual molecules cannot be distinguished from one another, analysis of that region cannot be performed, and the molecules in that region will not be included in the image. In principle, this should not happen since the density of *fluorescent* molecules is controlled by the relative rates of photoactivation and photobleaching, but in situations where full control over the density of fluorescent molecules is not achieved, regions with densities per unit area of active molecules above some maximum level will appear in the image to have fewer molecules than they actually have. This maximum density $D_{\max}$ within any given acquisition frame (the density in the final image will be much higher) can be estimated as $D_{\max} = 1/r_0^2$, which requires the density $D = N/A$ to be $D << D_{\max}$, where N is

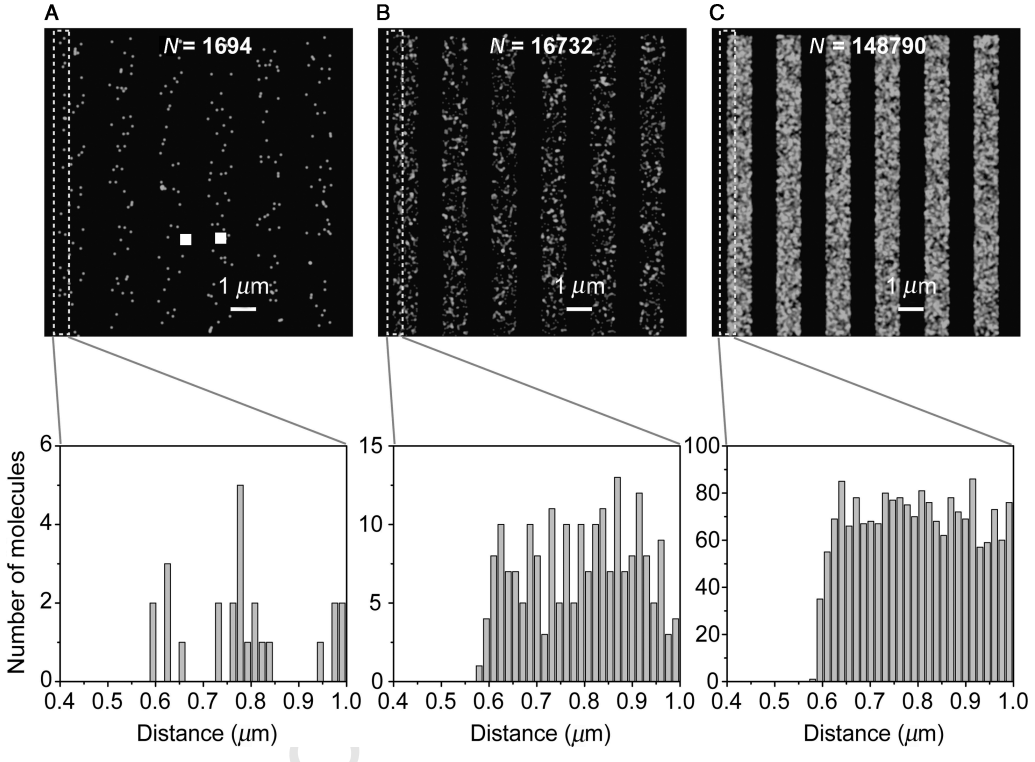

Fig. 9 Imaging of nanoscale structures requires a high density of localized molecules in addition to nanometer localization precision. The effect of the number of localized molecules on the fluorescence photoactivation localization microscopy (FPALM) image of a simulated patterned structure with ~1-μm wide strips in which all molecules reside is shown by zooming in on the edge of the strip. (upper row) Simulated FPALM images of (A) 1694 molecules, (B) 16732 molecules, and (C) 148790 molecules localized in a background-free area of ~12 × 12 μm. Molecular positions are plotted additively, weighted by the brightness of each individual molecule, the image of which was simulated to contain ~400 photons emitted at 520 nm and detected by a 1.2 NA (numerical aperture) lens with diffraction-limited resolution of 264 nm. (lower row) Histograms of the number of molecules localized within evenly spaced bins 15-nm wide show the lateral profile of the edge clearly for large numbers of molecules (right), but a limited number of molecules (left) limits the ability to discern the step, even though the localization precision was the same for all three cases (A–C).

the number of molecules within a region of area A, and r_0 is the radius of the point spread function. If the illumination is nonuniform, activation rates will be increased in areas with higher activation laser intensity, leading to higher densities of fluorescent molecules, while in regions with lower readout laser intensity molecules will be less likely to emit enough photons to be classified as above threshold. Thus, for quantitative characterization of molecular distributions, sample regions with a nearly uniform readout illumination profile are desirable. Nonuniform activation profile is less problematic as long as the density of molecules stays

below D_{max}, and as long as the acquisition lasts long enough to activate molecules within regions illuminated at lower readout intensity. Thus, one advantage of spreading the readout beam to a larger radius than the activation beam is to achieve a small but nearly uniformly illuminated central area within the field of view.

C. Failed Localization: Pixelization Artifacts

If molecules are imaged in samples with high background levels or if insufficient numbers of emitted photons are collected, the algorithm which fits a Gaussian to the image of the molecule may not reliably find the center of the molecule. In such cases, small changes in the initial coordinates for the fitting routine may produce large changes in the final coordinates obtained, or the coordinates obtained may end up at the edges of the allowed regions. FPALM images suffering from such a problem will show significant numbers of molecules falling on the edges of image pixels. This ''pixelization artifact'' can be remedied by checking whether initial coordinates for the fitting algorithm have a strong effect on final apparent molecular coordinates, by increasing thresholds to include only the brighter molecules, or in some cases by using a nonuniform background subtraction.

The technical factors which limit the rate of imaging are the readout and activation laser intensities, and the camera frame rate and noise properties. Fundamentally, the photoactivation quantum yield, photobleaching quantum yield, and the maximum fluorophore emission rate per molecule (e.g., at saturation) also limit acquisition rate because localization-based resolution depends on controlling the number of active molecules, detecting as many photons as possible in the shortest time possible, and photobleaching. However, once the utility of a method has been established, technological advances are often motivated, and new tools, such as improved PA markers, can be developed. The FPALM acquisition rate can in principle be increased significantly, given that camera frame rates can be increased without inducing prohibitively large readout noise, and given that sufficient photons can be detected from each molecule to provide a useful improvement in resolution. Based on estimated saturating intensities for enhanced green fluorescent protein (EGFP) and other GFPs, and current intensities used for cellular FPALM imaging, improvements in FPALM frame rate of at least tenfold are likely possible with current technology and PA-FPs. When active molecules remain fluorescent for several frames, Betzig *et al.* combine data from each frame to improve the number of detected photons per molecule (Betzig *et al.*, 2006), which is feasible in fixed samples where molecules are not moving during the acquisition.

D. Light Exposure

Exposure of living cells to laser radiation typically causes damage and alters biological function, especially at high intensities. In FPALM, the readout laser intensities used so far are of order $\sim$1000 W/cm^2. In confocal microscopy, from a

few μW up to $\sim$1 mW of power may illuminate the sample in a diffraction-limited focal area of $\sim$0.2 μm^2, yielding intensities as high as 5×10^5 W/cm^2 during the brief ($\sim$1 μs) dwell time within a given region. While the illumination in FPALM is continuous, and in the confocal illumination in a given region occurs once per scan (of order 1 μs per second), the dose received by the cells in these two methods is arguably similar for the following reason: in practice, during imaging by confocal microscopy, a significant fraction of fluorophores will photobleach during the time it takes to find a suitable sample, optimize microscope parameters, and acquire several images. Each photobleached fluorophore has a certain probability of generating reactive oxidative species, which can lead to cell damage. If N_B, the number of bleached fluorescent molecules in the focal plane of a confocal microscopy experiment is at least a few percent (here use 10%) of N_I, the initial number of molecules, and a probe concentration of $\sim$5 μM is present initially, one can estimate N_I if the focal plane is 0.6-μm thick and 200 μm $\times$ 200 μm in lateral extent with 20% coverage of regions by the probe. Using $N_I = C \cdot V_{illum}$ where C is the concentration of dye and V_{illum} is the volume illuminated during the scan, we find $N_I \sim 1.7 \times 10^7$ molecules, and $N_B \sim 1.7 \times 10^6$ molecules. In FPALM, the number of molecules bleached is similar to or greater than the number localized, neglecting a modest fraction of activated molecules which are not localized due to thresholds and a small number of pairs of molecules not localized because they are too close together. The number of localized molecules is typically 10^4–10^6 (Betzig *et al.*, 2006; Hess *et al.*, 2006), which is in the same range as or lower than the number of bleached molecules in a confocal experiment. Thus, it is expected that photodamage in FPALM experiments could be similar to that received during acquisition of a single frame-averaged confocal microscope image. However, only rigorous testing of effects on specific cell lines and specific biological processes will definitively answer this question.

E. Additional Single-Molecule Information Extracted by FPALM

In addition to the position map (image) which is obtained, FPALM also measures the number and brightness of individual molecules, information which is not available to standard imaging techniques. The distribution of fluorescence intensities can be a useful measure of probe performance, and can reveal population heterogeneities inaccessible to bulk measurements. Figure 10 shows fluorescence intensity histograms for PA-GFP, Dendra2-actin (Gurskaya *et al.*, 2006), and Dronpa (Ando *et al.*, 2004) expressed in fibroblast cells and imaged by FPALM, demonstrating information that would not be easily obtained in normal fluorescence microscopes unless the concentration of the probes were known. Please note that these data were not corrected for relative differences in excitation rate or detection efficiency, and should therefore not be considered a quantitative comparison among the three species. Furthermore, environmental variables such as probe dipole moment orientation, pH, membrane potential, ion concentration,

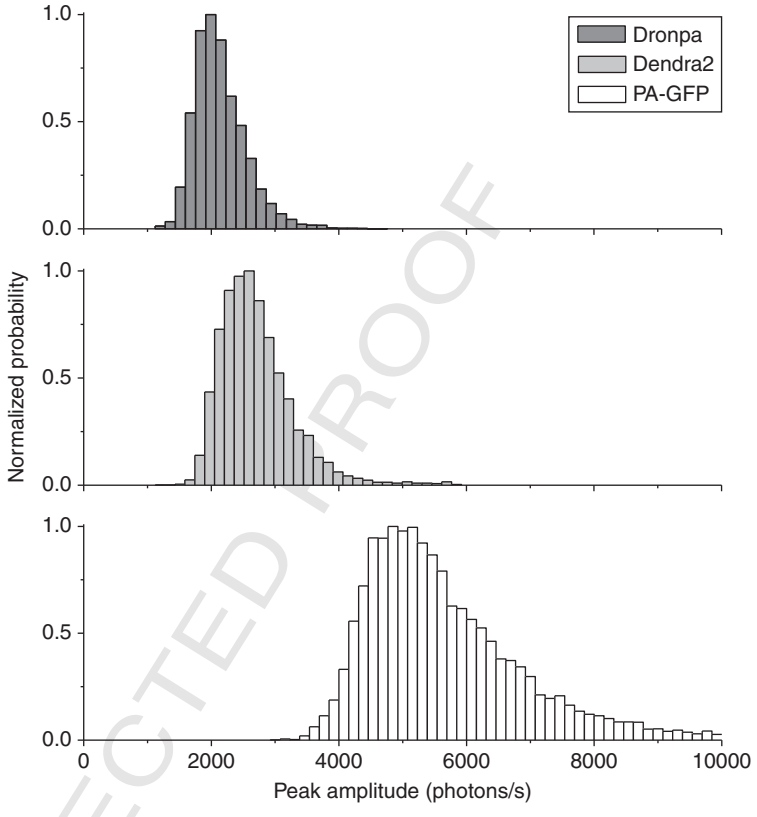

Fig. 10 Intensity distributions of many localized single molecules of the photoactivatable (PA) proteins Dronpa, Dendra2, and PA-GFP (green fluorescent protein) in fixed fibroblasts imaged by fluorescence photoactivation localization microscopy (FPALM). Since the results for each protein were obtained on different days, under differing excitation (readout) intensities, and have not been corrected for filter transmission, they do not provide a reliable comparison of relative brightness between different proteins, but they do demonstrate the ability to quantify the brightness of a variety of molecular species in cells using FPALM image data. Constructs and purified protein provided courtesy of Uli Nienhaus and Joerg Wiedenmann (Ulm), George Patterson (NIH), and Vladislav Verkhusha (Albert Einstein).

and local viscosity can change the spectral and photophysical characteristics of many fluorescent probes.

F. Future Directions

While a PA version of any protein with known sequence can in principle be produced, currently there are a limited number of PA-FPs (Gurskaya *et al.*, 2006; Lukyanov *et al.*, 2005). Those available are not easy to combine with other PA-FPs

because of spectral overlap. In particular, many of the red fluorescent PA-FPs are fluorescent in their preactivated state, and therefore prohibit use of that portion of the spectrum for another probe. For multicolor applications, PA-FPs which emit in the blue or far red portions of the spectrum and are nonfluorescent before activation are in demand.

Of considerable interest are values for the photoactivation quantum yields (Φ_{PA}) of existing probes. The value of Φ_{PA} is the probability that a molecule will be converted from its inactive (preactivation) form into its active form, given that it absorbed a photon. Furthermore, the total conversion yield, the fraction of a given population of PA-FPs that can ultimately be activated, is not known for any PA-FP. Such numbers are crucial for biological applications where it is desirable to image potentially rare molecular species, and for making quantitative comparisons between PA probes. For two-color imaging with a single activation laser, in the case of an inactive probe whose emission overlaps with the emission of the active form of a second probe, the relative magnitudes of Φ_{PA} will determine whether both probes can feasibly be used together.

Of course, since FPALM resolution ultimately depends on density of molecules and localization precision, probes are desired which emit as many photons as possible before photobleaching. Less obvious is the rate at which those photons are emitted, which should be as high as possible to minimize frame acquisition times for live-cell applications and improve contrast of molecules against inevitable background. Probe molecules must also have a finite photobleaching yield or a finite conversion yield back into the inactive state to allow control over the number of fluorescent molecules. Without such control, the number of fluorescent molecules will rapidly grow so large that individual molecules cannot be distinguished.

Multicolor FPALM is of considerable interest for a variety of biological applications. The ability to colocalize two molecular species at the nanometer length scale in a living cell has been long coveted. Two-species single-particle tracking experiments have already led to significant biological insights (Douglass and Vale, 2005). Two-color STED imaging has been demonstrated recently with <30 nm and $\sim$65-nm resolution for each probe, respectively (Donnert *et al.*, 2007). Unfortunately, for FPALM the available PA-FPs are so far difficult to use in concert, particularly because of spectral overlap between their (as many as four) emission spectra, and the increased number of excitation and activation wavelengths needed (as many as four in total). One potentially ideal combination would be two PA-FPs which emit only in their active forms, activate with the same wavelength, and read out with the same wavelength, but have nonoverlapping emission spectra. A bright red fluorescent PA-FP with high contrast ratio, $\sim$500-nm excitation, and $\sim$400-nm activation would be ideal. Perhaps slight modification of an existing red-emitting PA-FP would yield a good pair with PA-GFP or Dronpa. Alternatively, probes which emit at the same wavelength but have completely separable activation spectra are also feasible options.

VI. Summary

FPALM can image living or fixed biological samples with localization-based resolution well below the diffraction limit. Initially, nonfluorescent PA molecules are (1) activated in small numbers at a time, (2) imaged, and (3) photobleached or converted back to the inactive state. Steps 1–3 are then repeated to read out as many molecules as possible or as are desired. An image is then reconstructed by plotting the positions of each localized molecule, with intensity proportional to the number of detected photons from that molecule, and a size equal to the calculated or measured localization precision. Structures in living cells can be imaged with better than 40 nm localization-based resolution, depending on a number of factors, including photon emission rate per fluorophore, fluorescence background noise, diffusion coefficient of the labeled species, and acquisition time, which can be as fast as a few seconds.

Acknowledgments

The authors thank George Bernhardt, Scott Collins, and Patrick Swinney for the sapphire calibration sample, Joshua Zimmerberg and Paul Blank for the argon laser and CCD camera, Vladislav Verkhusha for the Dendra2 construct, Joerg Wiedenmann and Uli Nienhaus for EosFP constructs and purified protein, George Patterson for the PA-GFP construct, Sarah Maas and Kevin Mills for the PA-GFP-HA construct, Thomas Tripp for machining, Manasa Gudheti for assistance with cell culture, and Dean Astumian, Joerg Bewersdorf, and Sharon Ashworth for useful discussions. This work was supported by National Institutes of Health grant K25AI65459, National Science Foundation Grant CHE-0722759, and funds from the University of Maine Office of the Vice President for Research. T.G. benefited from a University of Maine Graduate Research Assistantship (UGRA).

References

Ando, R., Mizuno, H., and Miyawaki, A. (2004). Regulated fast nucleocytoplasmic shuttling observed by reversible protein highlighting. *Science* **306,** 1370–1373.

Betzig, E., and Trautman, J. K. (1992). Near-field optics—Microscopy, spectroscopy, and surface modification beyond the diffraction limit. *Science* **257,** 189–195.

Betzig, E., Patterson, G. H., Sougrat, R., Lindwasser, O. W., Olenych, S., Bonifacino, J. S., Davidson, M. W., Lippincott-Schwartz, J., and Hess, H. F. (2006). Imaging intracellular fluorescent proteins at nanometer resolution. *Science* **313,** 1642–1645.

Betzig, E., Trautman, J. K., Harris, T. D., Weiner, J. S., and Kostelak, R. S. (1991). Beating the diffraction barrier: Optical microscopy on a nanometer scale. *Science* **251,** 1468–1470.

Born, M., and Wolf, E. (1997). (''Principles of Optics: Electromagnetic Theory of Propagation, Interference and Diffraction of Light.'') Cambridge University Press, Cambridge, UK; New York.

Denk, W., Strickler, J. H., and Webb, W. W. (1990). 2-Photon laser scanning fluorescence microscopy. *Science* **248,** 73–76.

Dickson, R. M., Cubitt, A. B., Tsien, R. Y., and Moerner, W. E. (1997). On/off blinking and switching behaviour of single molecules of green fluorescent protein. *Nature* **388,** 355–358.

Donnert, G., Keller, J., Medda, R., Andrei, M. A., Rizzoli, S. O., Luhrmann, R., Jahn, R., Eggeling, C., and Hell, S. W. (2006). Macromolecular-scale resolution in biological fluorescence microscopy. *Proc. Natl. Acad. Sci. USA* **103,** 11440–11445.

Donnert, G., Keller, J., Wurm, C. A., Rizzoli, S. O., Westphal, V., Schonle, A., Jahn, R., Jakobs, S., Eggeling, C., and Hell, S. W. (2007). Two-color far-field fluorescence nanoscopy. *Biophys. J.* **92,** L67–L69.

Douglass, A. D., and Vale, R. D. (2005). Single-molecule microscopy reveals plasma membrane microdomains created by protein-protein networks that exclude or trap signaling molecules in T cells. *Cell* **121,** 937–950.

Gordon, M. P., Ha, T., and Selvin, P. R. (2004). Single-molecule high-resolution imaging with photobleaching. *Proc. Natl. Acad. Sci. USA* **101,** 6462–6465.

Gurskaya, N. G., Verkhusha, V. V., Shcheglov, A. S., Staroverov, D. B., Chepurnykh, T. V., Fradkov, A. F., Lukyanov, S., and Lukyanov, K. A. (2006). Engineering of a monomeric green-to-red photoactivatable fluorescent protein induced by blue light. *Nat. Biotechnol.* **24,** 461–465.

Gustafsson, M. G. (2005). Nonlinear structured-illumination microscopy: Wide-field fluorescence imaging with theoretically unlimited resolution. *Proc. Natl. Acad. Sci. USA* **102,** 13081–13086.

Gustafsson, M. G. L., Agard, D. A., and Sedat, J. W. (1999). I^5M: 3D widefield light microscopy with better than 100 nm axial resolution. *J. Microsc.* **195,** 10–16.

Heikal, A. A., Hess, S. T., Baird, G. S., Tsien, R. Y., and Webb, W. W. (2000). Molecular spectroscopy and dynamics of intrinsically fluorescent proteins: Coral red (dsRed) and yellow (Citrine) (vol 97, pg 11996, 2000). *Proc. Natl. Acad. Sci. USA* **97,** 14831–14831.

Hell, S. W. (2007). Far-field optical nanoscopy. *Science* **316,** 1153–1158.

Hell, S. W., Jakobs, S., and Kastrup, L. (2003). Imaging and writing at the nanoscale with focused visible light through saturable optical transitions. *Appl. Phys. A* **77,** 859–860.

Hell, S. W., and Wichmann, J. (1994). Breaking the diffraction resolution limit by stimulated emission: Stimulated-emission-depletion fluorescence microscopy. *Opt. Lett.* **19,** 780–782.

Hess, S. T., Girirajan, T. P., and Mason, M. D. (2006). Ultra-high resolution imaging by fluorescence photoactivation localization microscopy. *Biophys. J.* **91,** 4258–4272.

Hess, S. T., Heikal, A. A., and Webb, W. W. (2004). Fluorescence photoconversion kinetics in novel green fluorescent protein pH sensors. *J. Phys. Chem. B* **108,** 10138–10148.

Hess, S. T., and Webb, W. W. (2002). Focal volume optics and experimental artifacts in confocal fluorescence correlation spectroscopy. *Biophys. J.* **83,** 2300–2317.

Hofmann, M., Eggeling, C., Jakobs, S., and Hell, S. W. (2005). Breaking the diffraction barrier in fluorescence microscopy at low light intensities by using reversibly photoswitchable proteins. *Proc. Natl. Acad. Sci. USA* **102,** 17565–17569.

Kenworthy, A. K., Nichols, B. J., Remmert, C. L., Hendrix, G. M., Kumar, M., Zimmerberg, J., and Lippincott-Schwartz, J. (2004). Dynamics of putative raft-associated proteins at the cell surface. *J. Cell Biol.* **165,** 735–746.

Klar, T. A., Jakobs, S., Dyba, M., Egner, A., and Hell, S. W. (2000). Fluorescence microscopy with diffraction resolution barrier broken by stimulated emission. *Proc. Natl. Acad. Sci. USA* **97,** 8206–8210.

Lacoste, T. D., Michalet, X., Pinaud, F., Chemla, D. S., Alivisatos, A. P., and Weiss, S. (2000). Ultrahigh-resolution multicolor colocalization of single fluorescent probes. *Proc. Natl. Acad. Sci. USA* **97,** 9461–9466.

Lagerholm, B. C., Averett, L., Weinreb, G. E., Jacobson, K., and Thompson, N. L. (2006). Analysis method for measuring submicroscopic distances with blinking quantum dots. *Biophys. J.* **91,** 3050–3060.

Levi, V., Ruan, Q., and Gratton, E. (2005a). 3-D particle tracking in a two-photon microscope: Application to the study of molecular dynamics in cells. *Biophys. J.* **88,** 2919–2928.

Levi, V., Ruan, Q., Plutz, M., Belmont, A. S., and Gratton, E. (2005b). Chromatin dynamics in interphase cells revealed by tracking in a two-photon excitation microscope. *Biophys. J.* **89,** 4275–4285.

Lidke, K. A., Rieger, B., Jovin, T. M., and Heintzmann, R. (2005). Superresolution by localization of quantum dots using blinking statistics. *Opt. Express* **13,** 7052–7062.

Liu, Z., Lee, H., Xiong, Y., Sun, C., and Zhang, X. (2007). Far-field optical hyperlens magnifying sub-diffraction-limited objects. *Science* **315,** 1686.

Lukyanov, K. A., Chudakov, D. M., Lukyanov, S., and Verkhusha, V. V. (2005). Photoactivatable fluorescent proteins. *Nat. Rev. Mol. Cell Biol.* **6,** 885–891.

Moerner, W. E., Peterman, E. J., Sosa, H., Brasselet, S., Dickson, R. M., Kummer, S., Sakowicz, R., and Goldstein, L. S. B. (1999). Single-molecule studies of fluorescent proteins and enzymes. *Biophys. J.* **76,** A20–A20.

Pawley, J. B. (1995). (''Handbook of Biological Confocal Microscopy.'') Plenum Press, New York.

Ponti, A., Matov, A., Adams, M., Gupton, S., Waterman-Storer, C. M., and Danuser, G. (2005). Periodic patterns of actin turnover in lamellipodia and lamellae of migrating epithelial cells analyzed by quantitative fluorescent speckle microscopy. *Biophys. J.* **89,** 3456–3469.

Qu, X. H., Wu, D., Mets, L., and Scherer, N. F. (2004). Nanometer-localized multiple single-molecule fluorescence microscopy. *Proc. Natl. Acad. Sci. USA* **101,** 11298–11303.

Rust, M. J., Bates, M., and Zhuang, X. (2006). Sub-diffraction-limit imaging by stochastic optical reconstruction microscopy (STORM). *Nat. Methods* **3,** 793–796.

Salmon, W. C., Adams, M. C., and Waterman-Storer, C. M. (2002). Dual-wavelength fluorescent speckle microscopy reveals coupling of microtubule and actin movements in migrating cells. *J. Cell Biol.* **158,** 31–37.

Sandison, D. R., Piston, D. W., Williams, R. M., and Webb, W. W. (1995). Quantitative comparison of background rejection, signal-to-noise ratio, and resolution in confocal and full-field laser-scanning microscopes. *Appl. Opt.* **34,** 3576–3588.

Sandison, D. R., and Webb, W. W. (1994). Background rejection and signal-to-noise optimization in confocal and alternative fluorescence microscopes. *Appl. Opt.* **33,** 603–615.

Schrader, M., and Hell, S. W. (1996). 4PI-confocal images with axial superresolution. *J. Microsc.* **183,** 189–193.

Sharonov, A., and Hochstrasser, R. M. (2006). Wide-field subdiffraction imaging by accumulated binding of diffusing probes. *Proc. Natl. Acad. Sci. USA* **103,** 18911–18916.

Shvartsman, D. E., Kotler, M., Tall, R. D., Roth, M. G., and Henis, Y. I. (2003). Differently anchored influenza hemagglutinin mutants display distinct interaction dynamics with mutual rafts. *J. Cell Biol.* **163,** 879–999.

Waterman-Storer, C. M., Desai, A., Bulinski, J. C., and Salmon, E. D. (1998). Fluorescent speckle microscopy, a method to visualize the dynamics of protein assemblies in living cells. *Curr. Biol.* **8,** 1227–1230.

Xu, C., Zipfel, W., Shear, J. B., Williams, R. M., and Webb, W. W. (1996). Multiphoton fluorescence excitation: New spectral windows for biological nonlinear microscopy. *Proc. Natl. Acad. Sci. USA* **93,** 10763–10768.

Yildiz, A., Forkey, J. N., McKinney, S. A., Ha, T., Goldman, Y. E., and Selvin, P. R. (2003). Myosin V walks hand-over-hand: Single fluorophore imaging with 1.5-nm localization. *Science* **300,** 2061–2065.

Au4